OXFORD

Human Molecular Genetics, 2017, Vol. 26, No. 13 2386–2397

doi: 10.1093/hmg/ddx127
Advance Access Publication Date: 31 March 2017
Original Article

ORIGINAL ARTICLE

Loss of dynein-2 intermediate chain Wdr34 results in defects in retrograde ciliary protein trafficking and Hedgehog signaling in the mouse

Chuanqing Wu[1,2], Jia Li[2,3], Andrew Peterson[4], Kaixiong Tao[1,*], and Baolin Wang[2,5,*]

[1]Department of Gastrointestinal Surgery, Union Hospital, Tongji Medical College, Huazhong University of Science and Technology, Wuhan 430030, Hubei, China, [2]Department of Genetic Medicine, Weill Medical College of Cornell University, W404, New York, NY 10065,USA, [3]Institute of Biological Sciences and Biotechnology, Donghua University, Shanghai 201620, China, [4]Department of Molecular Biology, Genentech, South San Francisco, CA 94080, USA and [5]Department of Cell and Developmental Biology, Weill Medical College of Cornell University, W404, New York, NY 10065, USA

*To whom correspondence to be addressed at: 1300 York Avenue, W404, New York, NY 10065, USA. Tel: 212 7465357; Fax: 212 7468318; Email: baw2001@med.cornell.edu (B.W.); Email: tao_kaixiong@163.com (K.T.)

Abstract

The *Wdr34* gene encodes an intermediate chain of cytoplasmic dynein 2, the motor for retrograde intraflagellar transport (IFT) in primary cilia. Although mutations in human *WDR34* have recently been reported, the association of *WDR34* function with Hedgehog (Hh) signaling has not been established, and actual cilia defects in the *WDR34* mutant cells have also not been completely characterized. In the present study, we show that *Wdr34* mutant mice die in midgestation and exhibit open brain and polydactyly phenotypes. Several Hh-dependent ventral neural cell types are not specified in the mutant neural tube. The expression of the direct Hh targets, *Gli1* and *Patched 1*, is inhibited, while the expression of limb patterning genes that are normally inhibited by the Gli3 repressor is anteriorly expanded in mutant limbs. Comparison of cilia phenotype and function among wild type, *Dnchc2* (dynein 2 heavy chain), and *Wdr34* mutant cells demonstrates that cilia in both *Dnchc2* and *Wdr34* mutant cells are stumpy. Several ciliary proteins examined abnormally accumulate in the cilia of both mutant cells. Consistent with its function, overexpressed Wdr34 is occasionally localized to cilia, and Wdr34 is required for the ciliary localization of dynein 2 light intermediate chain Lic3. More interestingly, we show that both Dnchc2 and Wdr34 act between Smo and Gli2/Gli3 in the Hh pathway. Therefore, like Dnchc2, Wdr34 is required for ciliogenesis, retrograde ciliary protein trafficking, and the regulation of Gli2/Gli3 activators and repressors. Furthermore, both Wdr34 and Dnchc2 promote microtubule growth, a novel dynein 2 function in a non-cilia structure.

Introduction

The family of secreted Hedgehog (Hh) molecules plays an important role in the development of the central nervous system, limb, and many other structures in vertebrates (1). Hh signaling is initiated by the binding of Hh ligand to its cell surface receptor, Patched (Ptch), a twelve-pass membrane protein (2,3). This binding prevents Ptch from inhibiting Smoothened (Smo), a G-protein coupled receptor, allowing the Hh pathway

Received: December 29, 2016. **Revised:** March 25, 2017. **Accepted:** March 28, 2017

to be activated. Smo then transmits signals to activate the downstream Gli transcription factors. Of three Gli family members, Gli2 and Gli3 primarily mediate Hh signaling. In the absence of Hh signaling, Gli2 and Gli3 full-length proteins ($Gli2^{FL}$ and $Gli3^{FL}$) are proteolytically processed to generate C-terminally truncated transcriptional repressors ($Gli2^{Rep}$ and $Gli3^{Rep}$) (4,5). Hh signaling inhibits the proteolytical processing and converts the latent full-length proteins into activators, which subsequently activate the downstream transcriptional targets. Interestingly, one of these targets is *Gli1*, which serves to further enforce the Hh pathway activation, while *Ptch1* is another target to establish a negative feedback regulation of the pathway.

It is generally accepted that vertebrate Hh signaling occurs in the primary cilium, a solitary microtubule-based organelle that protrudes from the cell surface and functions in transducing extracellular signals (6). Consistent with this, the Hh pathway core components, including Ptch1, Smo, Gli2 and Gli3 proteins, Sufu, and Kif7, are localized to the cilia (7–11). Ciliary defects cause a diverse array of developmental abnormalities, such as polydactyly, central nervous system defects, polycystic kidney disease, respiratory and visual disorders, hydrocephalus, obesity, and mental retardation, which are collectively termed 'ciliopathies' (12).

Primary cilia originate from the mother centrioles, which serve as a basal body and a docking station for ciliary microtubules and intraflagellar transport (IFT) machinery during primary cilia elongation. IFT machinery is also essential for the maintenance of primary cilia. There are two IFT protein complexes, IFT-A and IFT-B. IFT-B, together with a kinesin 2 motor, is responsible for anterograde ciliary trafficking of protein complexes and vesicles, while IFT-A, together with a cytoplasmic dynein 2 motor, is responsible for retrograde ciliary protein and vesicle trafficking (13,14). There are several kinesin 2 motors that power anterograde ciliary trafficking (15). In contrast, cytoplasmic dynein 2 is currently the only known retrograde IFT motor in cilia. Dynein 2 in metazoans consists of a dimer of heavy chain subunits (encoded by *Dnchc2*, also known as *Dync2h1*, *Dhc1B*, or *Dhc2*), which associate with intermediate chains, light intermediate chains, and light chains (16–18). Mutations in mouse *Dnchc2* results in stumpy cilia and Hh signaling defect (19,20), and mutations of human *DYNC2H1* gene also cause short-rib polydactyly syndrome type III (21). Similarly, mutations in human *WDR34* gene, which is recently shown to encode a dynein 2 intermediate chain (16), also result in short-rib polydactyly syndrome type III (22,23). Human *WDR34* mutant fibroblasts exhibit short and bulbous cilia. However, neither has it been established whether *WDR34* mutations affect Hh signaling, nor has the mouse *Wdr34* mutant phenotypes been reported.

In this study, we show that loss of *Wdr34* in mice results in stumpy cilia and abnormal accumulation of ciliary proteins in cilia. *Wdr34* mutant mice exhibit open brain and polydactyly phenotypes. Nevertheless, although $Gli2^{FL}$ and $Gli3^{FL}$ levels are increased in the mutant, they are not activated, as the expression of Hh targets that is dependent on activated $Gli2^{FL}$ and $Gli3^{FL}$ is inhibited. On the other hand, the expression of the limb patterning genes that are normally inhibited by $Gli3^{Rep}$ are anteriorly expanded in the mutant limb bud, suggesting that $Gli3^{Rep}$ function is also attenuated. We also show that Wdr34 acts between Smo and Gli2/Gli3 in the Hh pathway. Thus, our study links *Wdr34* function to Hh signaling, ciliogenesis, and retrograde ciliary trafficking.

Results

Loss of *Wdr34* impairs Hh signaling in mice

To determine the role of *Wdr34 in vivo*, we used the targeted gene homologous recombination approach to mutate the gene by deleting exons 3–8 in mice (Fig. 1A and B). The deletion of the exons, which cover most of the coding region, is expected to cause an open reading frame shift, thus most likely resulting in a null allele. The vast majority of mice homozygous for the *Wdr34* mutation died in midgestation varying from embryonic day 10.5 to 12.5 (E10.5 –E12.5), occasionally surviving until E16.5. The mutant embryos exhibited open brain, spinal bifida, microphthalmia, and polydactyly (Fig. 1C and D).

Given the role of Hh signaling in the central nervous system, eye, and limb development, we next characterized the neural tube phenotype of the mutant in more detail. The generation of all five types of ventral neural progenitors in the developing neural tube is induced by different concentrations of Sonic Hedgehog (Shh) that is expressed in the notochord and the floor plate, while the dorsal neural progenitor specification is inhibited by Shh signaling. These different types of neural progenitors can be marked by the expression of specific transcription factors (24). We thus examined the expression of several neural tube markers in *Wdr34* wild type and mutant neural tube of E10.5 embryos by immunofluorescence. In wild type neural tube, Foxa2, Nkx2.2, and Hb9 and Isl1 label the floor plate, V3 progenitors, and motor neurons, respectively. However, all these ventral markers were absent in the *Wdr34* mutant neural tube. In contrast, Pax6 expression, which is normally ventrally restricted by the high Shh signaling, expanded throughout the entire ventral neural tube. Similarly, dorsal marker Pax7 expression domain was also slightly ventrally extended. On the other hand, loss of *Wdr34* does not affect Shh expression in the notochord, indicating that a lack of the ventral neural tube markers' expression was due to defective Hh signal transduction but not Shh expression (Fig. 2A).

To determine whether inactivation of *Wdr34* directly affects Hh signaling, we examined the expression of *Ptch1*, a transcriptional target of Hh signaling. To this end, the *Wdr34* mutant allele was crossed into $Ptch1^{lacZki}$ heterozygous mutant, in which the *lacZ* gene is inserted in the *Ptch1* locus so that lacZ expression is an indicator of *Ptch1* expression (25). As predicated, lacZ was expressed in brain, spinal cord, and limb buds of wild type E10.5 embryos, but not in those of *Wdr34* mutants (Fig. 2B). Similarly, *in situ* hybridization results showed that the expression of both *Ptch1* and *Gli1*, another Hh target, was detected only in wild type but not the mutant limb buds, though *Shh* expression was unaffected (Fig. 3).

To determine the molecular basis of the polydactyly phenotype of the *Wdr34* mutant, we examined expression of several limb-patterning genes that are regulated by Hh signaling. *Gremlin*, *Hand2*, *Hoxd11*, and *Hoxd13* expression was normally restricted to the posterior region of developing limbs by $Gli3^{Rep}$ (26–29). However, the expression of all these genes was anteriorly expanded in the mutant limbs. Similarly, the expression of both *Fgf4* and *Fgf8* in the apical ectodermal ridge (AER), which is also restricted by $Gli3^{Rep}$ (30), was anteriorly extended in the mutant limb as compared to wild type (Fig. 3).

To correlate the mutant phenotypes with Gli2 and Gli3 functions, we examined Gli2 protein levels and Gli3 processing in *Wdr34* mutant embryos by immunoblotting with Gli2 and Gli3 antibodies (5,31). The results showed that levels of both $Gli2^{FL}$ and $Gli3^{FL}$ were increased in the mutant, while $Gli3^{Rep}$ levels

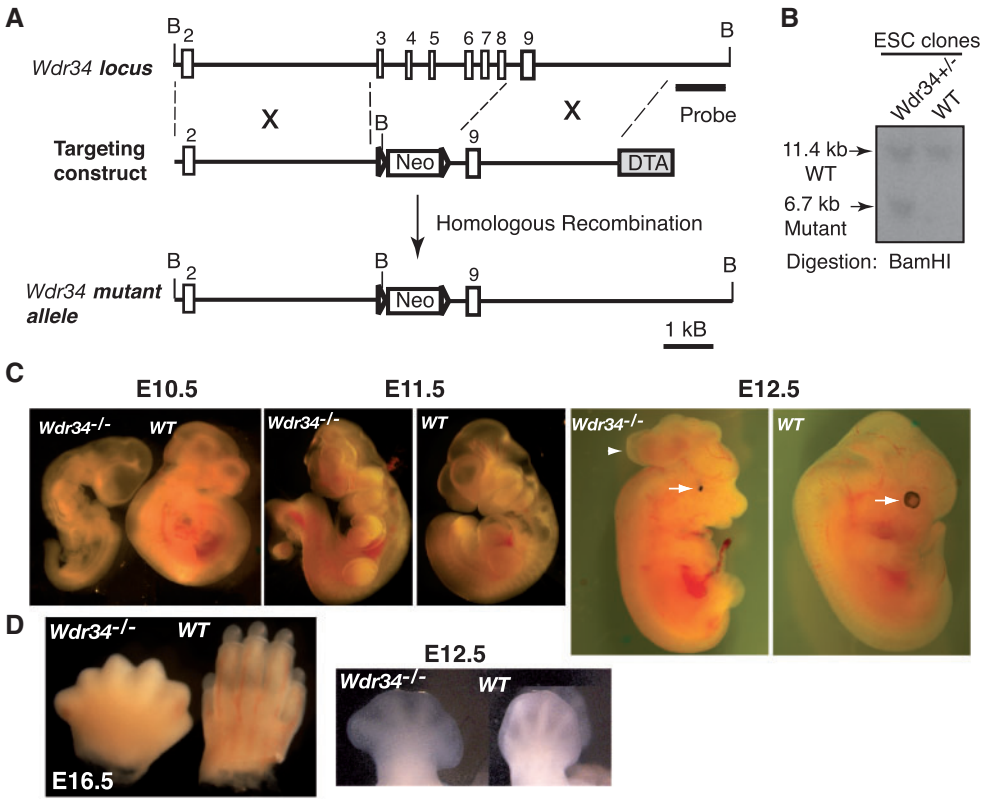

Figure 1. Inactivation of *Wdr34* results in open brain, polydactyly, and microphthalmia in mice. (**A**) The gene targeting strategy used to create a mouse *Wdr34* mutant allele. Open rectangles are referred to as exons and lines as introns. Probe and BamHI restriction sites used for Southern blot are shown. Triangle, loxP site; Neo, neomycin; DTA, diphtheria toxin A. (**B**) Southern blot of representative mutant and wild type (wt) ES cell clones. (**C**) The morphology of wt and *Wdr34* mutant embryos at different developmental stages. Note the delayed development, open brain (pointed by arrowhead), and microphthalmia (indicated by arrow) of mutant embryos. (**D**) Limb phenotypes of E16.5 and E12.5 wt and mutant embryos. Note that E12.5 mutant limb paddle is wider than that of wt, indicating polydactyly.

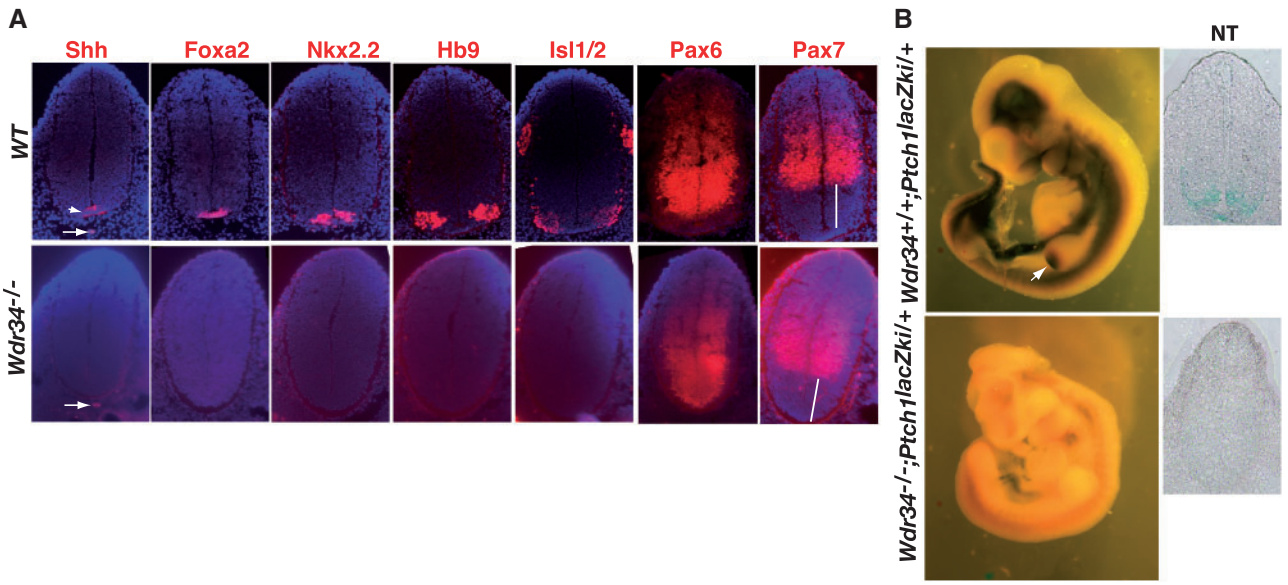

Figure 2. Inactivation of *Wdr34* disrupts Shh-dependent neural patterning in the neural tube and inhibits Hh signaling. (**A**) Ventral neural progenitors are not specified in the *Wdr34* mutant neural tube. E10.5 neural tube sections were immunostained for the indicated protein markers (red) and counterstained with DAPI for nuclei (blue). Note that none of the ventral markers was detected in the mutant, while the expression of dorsal markers (Pax6 and Pax7) was ventrally expanded. The two equal long lines are used to compare the length of ventral region lacking Pax7 expression in wt and the mutant, which is slightly shorter in the mutant. Arrowhead and arrow indicate Shh expression in the floor plate and notochord, respectively. (**B**) *Ptch1-lacZ* expression is undetectable in the mutant. E10.5 embryos with indicated genotypes were subject to lacZ staining. Transverse neural tube sections are shown to the right.

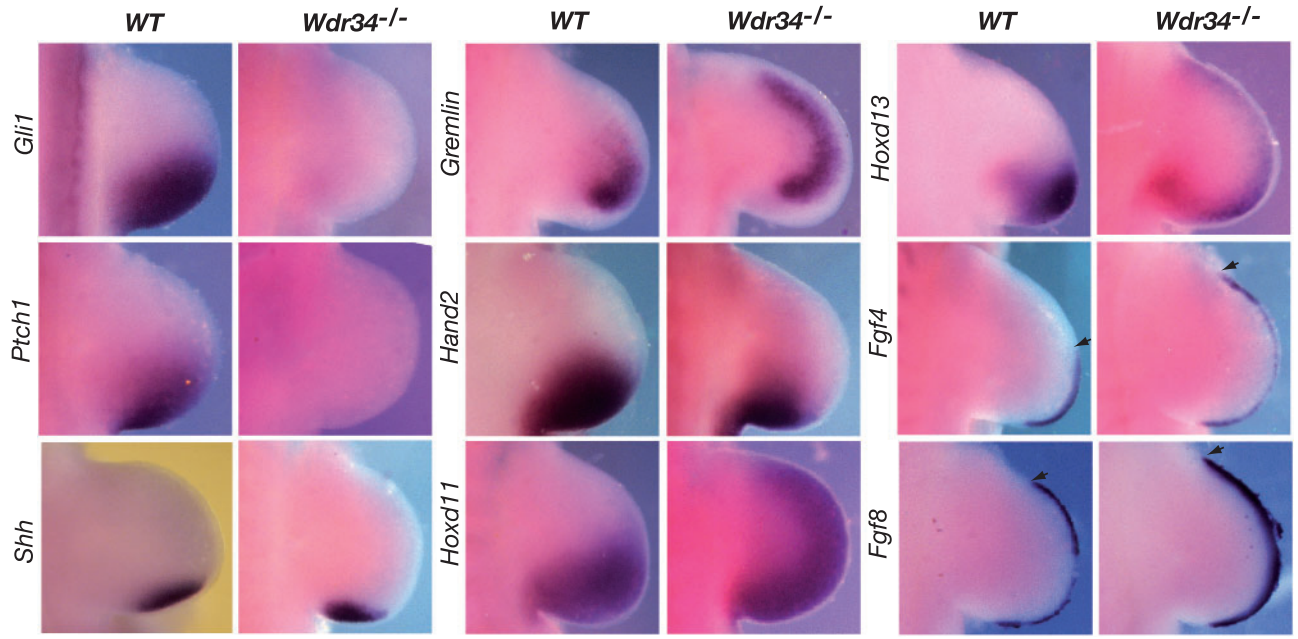

Figure 3. Altered expression of limb patterning genes in *Wdr34* mutant limb buds. Whole mount in situ hybridization of E10.5 limb buds shows the expression of limb patterning genes. Note that *Ptch1* and *Gli1* expression is not detected, while Shh is normally expressed in the mutant. The expression of the genes that are normally inhibited by Gli3 repressor is anteriorly expanded (*Gremlin*, *Hand2*, *Hoxd11*, *Hoxd13*, *Fgf4*, and *Fgf8*). Note that although the higher expression domain of *Hand2* in the mutant limb is smaller than that in WT limb, the weak expression is anteriorly expanded. Arrows indicate the anterior end of *Fgf4* and *Fgf8* expression.

were reduced (Fig. 4). Quantitative analysis showed that the $Gli3^{FL}$ to $Gli3^{Rep}$ ratio in the mutant is markedly increased as compared to that of wild type (graph in Fig. 4). Thus, Gli3 processing is reduced in the *Wdr34* mutant. Since the ventral neural tube patterning is primarily dependent on Gli2/Gli3 activators, whereas limb patterning mostly relies on the $Gli3^{Rep}$, these results indicate that both the Gli2/Gli3 activator and repressor functions are impaired in the *Wdr34* mutant.

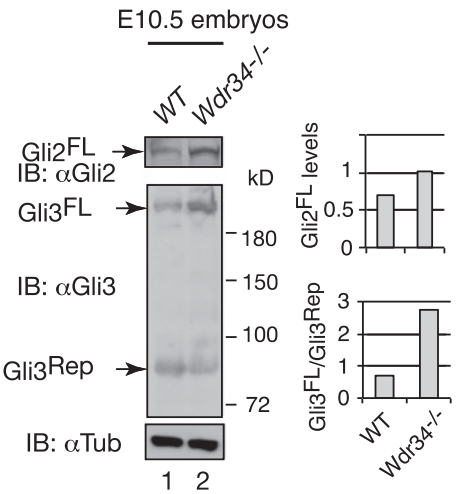

Figure 4. Western blots show the increase in $Gli2^{FL}$ and $Gli3^{FL}$ levels and decrease in $Gli3^{Rep}$ levels in E10.5 *Wdr34* mutant embryos. Tubulin blot is a loading control. Quantitative analysis of the Western blot results is shown by graphs to the right.

Loss of *Wdr34* and Dnchc2 results in stumpy cilia and defects in retrograde ciliary trafficking

Given that cilia are required for Hh signaling and Wdr34 is an intermediate chain of dynein 2, we next examined the cilia morphology by scanning electron microscopy (SEM). Cilia were long and thin in neuroepithelial cells in the lumen of the wild type neural tube, but short and swollen in the *Wdr34* mutant (Fig. 5A). Immunofluorescent staining for cilia markers, Arl13b and acetylated tubulin, showed that cilia density in both neuroepithelia of the neural tube and limb mesenchyme of the mutant was similar to that in wild type. However, the staining in wild type limb mesenchymal cells was usually elongated, but dotted in the mutant, indicating that cilia in the mutant cells are short and stumpy (Fig. 5B). Consistent with this, cilia in the mutant MEFs were significantly shorter than those in wild type. Cilia number in the mutant MEFs was also significantly lower than that in wild type MEFs (Fig. 5C, upper and middle graphs). These results suggest that Wdr34 is required for ciliogenesis and maintenance of cilia length.

Given that cytoplasmic dynein 2 is the motor for retrograde IFT in cilia, it is expected that loss of *Wdr34* function would lead to abnormal accumulation of ciliary proteins in cilia. To test this prediction, we examined and compared ciliary localization of several proteins in wild type, *Wdr34*, and *Dnchc2* mutant MEFs by immunofluorescence. Both Arl13b and Smo, two ciliary membrane proteins (7,32), were distributed evenly along cilia in wild type cells. However, they accumulated at the tip of the cilia in both *Wdr34* and *Dnchc2* mutant cells. Similarly, Ift88, Ift57, and Ift140, which represent IFT-B and IFT-A complexes (13), respectively, were also significantly enriched in the cilia of the mutant cells (Fig. 5C, images and lower graph). It is worth noting that primary cilia shaft is made of 9 microtubule triplet in the basal body, doublet in most part of cilia, and singlet at the cilia tip (14). Thus, the staining for acetylated tubulin at the cilia tip is often pointier than that in the main part and proximal end of cilia. This becomes especially apparent in *Wdr34* and *Dnchc2* mutants, as cilia assembly is defective in the mutants (Fig. 5C,

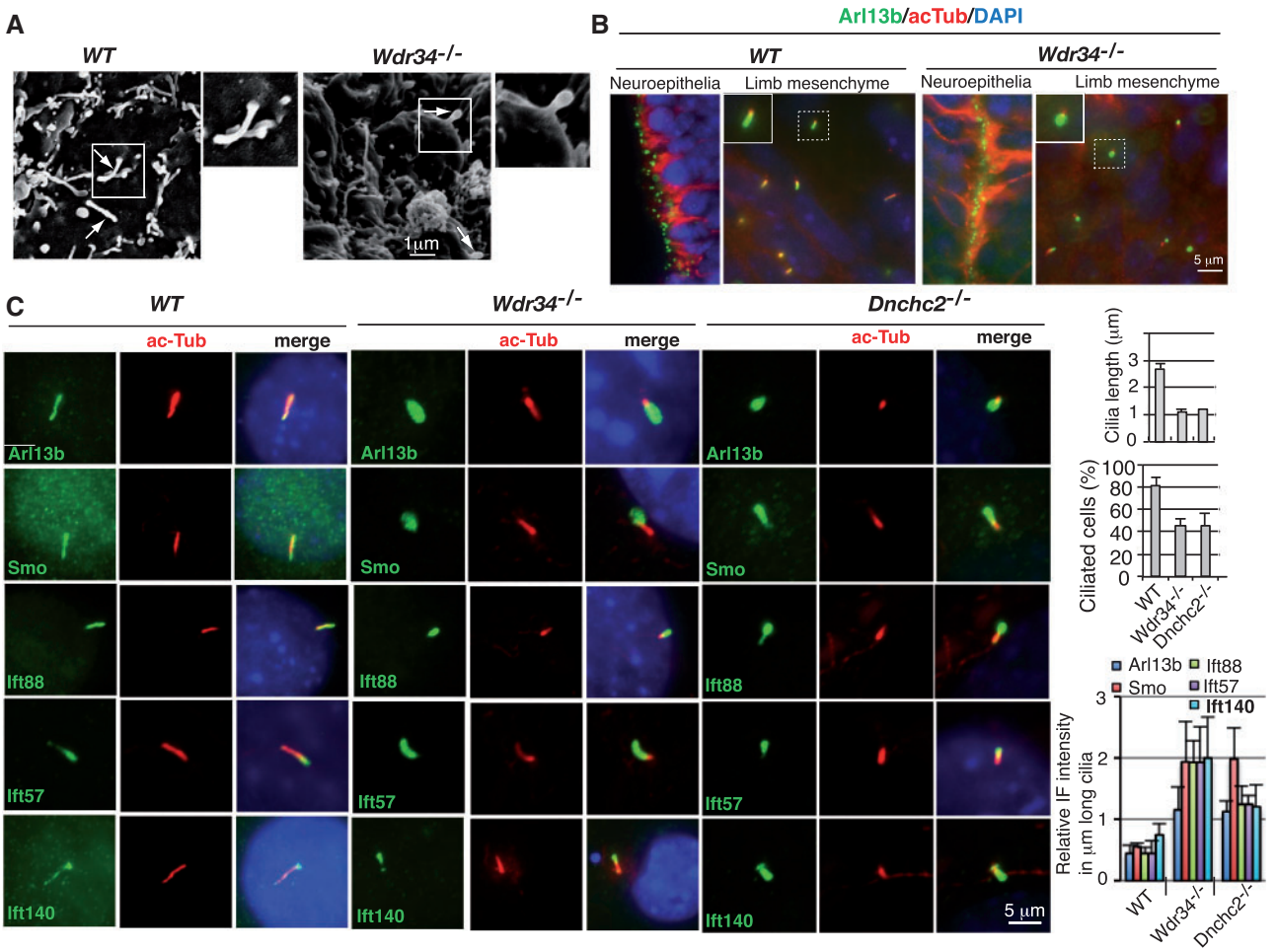

Figure 5. Stumpy cilia and aberrant accumulation of ciliary proteins in the cilia of *Wdr34* mutant cells. (**A**) Scanning electron microscopy (SEM) of the cilia of neural epithelia in the neural tube of E9.5 embryos. Arrows indicate cilia, and the enlargement of framed cilia is shown to the right. (**B**) The neural tube and limb mesenchyme of E10.5 embryos and (**C**) MEFs were immunostained for the indicated proteins, acetylated tubulin (ac-Tub), and nuclei (DAPI, blue). For Smo ciliary localization, cells were treated with ShhN conditioned medium 24h prior to immunostaining. Quantitative analysis of the results in C is shown by graphs to the right. Two-tailed Student t-test shows that all p-values are equal to or less than 0.0005 (upper graph), 0.0014 (middle graph), and 0.013 (lower graph), all of which are less than 0.05, thus significant. Note that cilia in the mutant cells are short and swollen and that all ciliary proteins examined accumulate abnormally at the cilia tip of both *Wdr34* and *Dnchc2* mutant cells. The pointy end of ac-Tub staining is the distal end of cilia.

images with the acetylated tubulin staining in the mutant cells). Since Arl13b, Smo, Ift88, Ift57, and Ift140 all localize to the pointy end of the mutant cilia, we conclude that they accumulate at the distal tip of cilia. Thus, like *Dnchc2* mutations (20,33), loss of *Wdr34* disrupts retrograde ciliary protein trafficking.

Because cilia number is significantly reduced in *Wdr34* mutant MEFs, we also wondered whether loss of *Wrd34* would affect the centriolar localization of several centrosomal proteins. Of four proteins examined, Cep164, Odf2, Ta3, and Cep290 (34–38), none appeared to be affected, suggesting that the basal body is normally assembled in the mutant cells (Fig. 6).

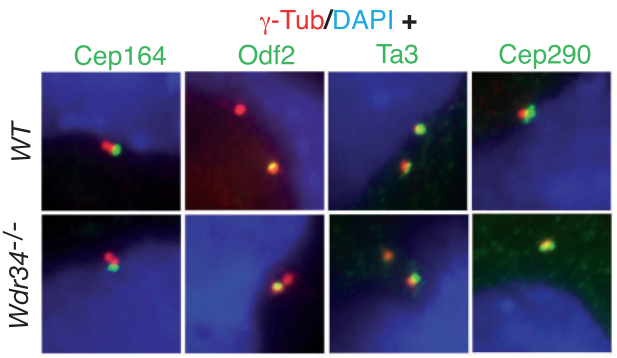

Figure 6. Normal localization of centrosomal proteins in *Wdr34* mutant cells. Wild type and *Wdr34* mutant MEFs were coimmunostained for the indicated proteins, γ-tubulin, and nuclei (DAPI, blue).

Wdr34 acts between smo and Gli2/Gli3 in the Hh pathway

Hh stimulation leads to accumulation of Smo, Gli2, and Gli3 in cilia (7,9,11). To determine at which step in the Hh pathway that *Wdr34* mutation acts, we tested whether Smo, Gli2, and Gli3 accumulated in the cilia of *Wdr34* and *Dnchc2* mutant cells in response to Hh stimulation. Both wild type and the mutant MEFs were incubated with ShhN conditioned medium prior to immunostaining for Smo, Gli2, or Gli3 together with acetylated tubulin. In the absence of ShhN stimulation, Smo was basically undetectable in the cilia of wild type cells we used, but detectable in about 50% and 20% of *Wdr34* and *Dnchc2* mutant cilia,

respectively. This is consistent with the finding that loss of *Dnchc2* function results in accumulation of Smo in cilia (33). Stimulation with ShhN significantly increased the percentage of Smo positive cilia in both wild type and mutant cells (Fig. 7, upper graph), indicating that loss of either *Wdr34* or *Dnchc2* does not impair the Smo accumulation in cilia. In contrast, Gli2 and Gli3 already accumulated in the cilia of the mutant cells without ShhN stimulation, and ShhN stimulation resulted in no further increase in Gli2 and Gli3 positive cilia number in the mutant cells, although it did in wild type cells (Fig. 7). This indicates that the loss of either *Wdr34* or *Dnchc2* gene function prevents Hh-dependent Gli2 and Gli3 accumulation in cilia. Thus, Wdr34 and Dnchc2 act downstream of Smo and upstream of Gli2/Gli3 in the Hh pathway. This is consistent with genetic evidence showing that ciliary genes act between Smo and Gli2 and Gli3 (6).

Subcellular localization of *Wdr34* and its role in the ciliary localization of other subunits of the dynein 2 complex

To determine the subcellular localization of Wdr34, wild type MEFs stably expressing green fluorescent protein (GFP) tagged Wdr34, Wdr34-GFP, were selected and subjected to immunofluorescence for GFP and acetylated tubulin. Wdr34-GFP was localized to cilia in only a small number (12%, $n = 35$) of Wdr34-GFP expressing cells. In most cells, Wdr34-GFP appeared to be concentrated in cell cortices and filopodia-like structures. This localization is specific since GFP alone was not localized to those structures (Fig. 8A).

Wdr34 contains five WD-repeats in its C-terminus. To map the region responsible for Wdr34 ciliary localization, the N- and C-terminal regions of Wdr34 were separately fused to GFP to create GFP-Wdr34-1-220 and GFP-Wdr34-221-E expression constructs, respectively. Immunostaining of MEFs expressing these two fusion proteins showed that GFP-Wdr34-1-220 was localized to cilia in some of the GFP-WDR34-1-220 expressing cells, while GFP-WDR34-221-E was diffusely localized to the cytoplasm (Fig. 8A). These data suggest that the N-terminus controls Wdr34 ciliary localization.

The cytoplasmic dynein 2 consists of heavy chain, intermediate chain, light intermediate chain, and light chain (16). Both the heavy chain Dnchc2 and light intermediate chain Lic3 are localized to cilia (39). Given that Wdr34 is a dynein 2 intermediate chain, we were curious about whether loss of Wdr34 affected Dnchc2 and Lic3 localization to cilia. As expected, both Dnchc2 and Lic3 were localized to cilia in wild type MEFs. However, while Dnchc2 remained in the cilia of *Wdr34* mutant cells, Lic3 did not (Fig. 8B). This suggests that Wdr34 is required for Lic3 ciliary localization and/or protein stability.

Delayed microtubule regrowth in *Wdr34* and Dnchc2 mutant cells

Given that dynein 2 is a retrograde IFT motor along cilium axoneme, a microtubule-based structure, we were also curious about whether loss of dynein 2 affects cytoplasmic microtubule growth and dynamics. The microtubule network in both *Wdr34* and *Dnchc2* mutant cells was similar to that in wild type cells

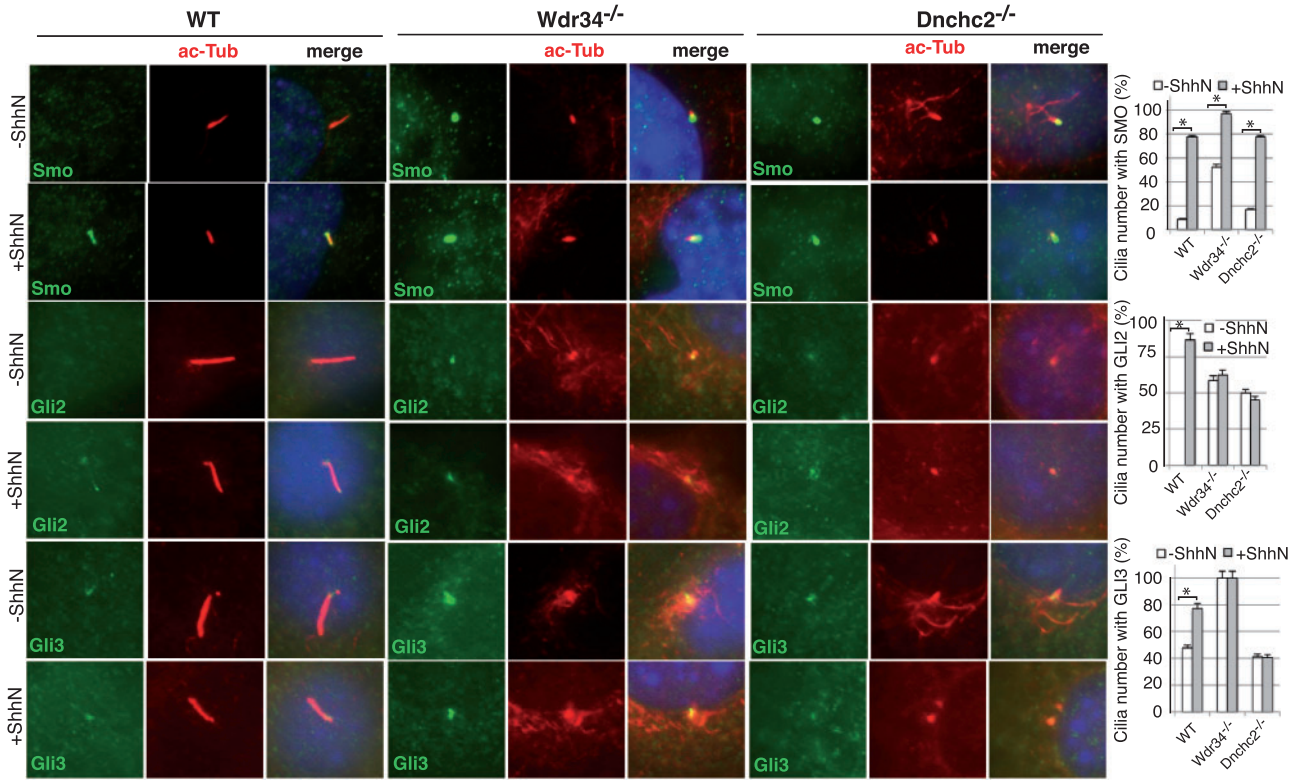

Figure 7. Wdr34 and Dnchc2 act between Smo and Gli2/Gli3 in the Hh pathway. WT, *Wdr34*, and *Dnchc2* mutant MEFs were immunostained with the indicated antibodies. The cilia number with or without detectable Smo, Gli2, or Gli3 were counted. Graphs to the right show percent cilia with Smo, Gli2, or Gli3 from at least 50 cilia in three different experiments. The p-values for those bar graphs marked with asterisks are equal to or less than 0.0015 (two-tailed Student t-test). Since they are less than 0.05, the difference between –ShhN and +ShhN is significant. Note that the ciliary localization of Smo but not Gli2 or Gli3 in mutant cells responded to ShhN stimulation.

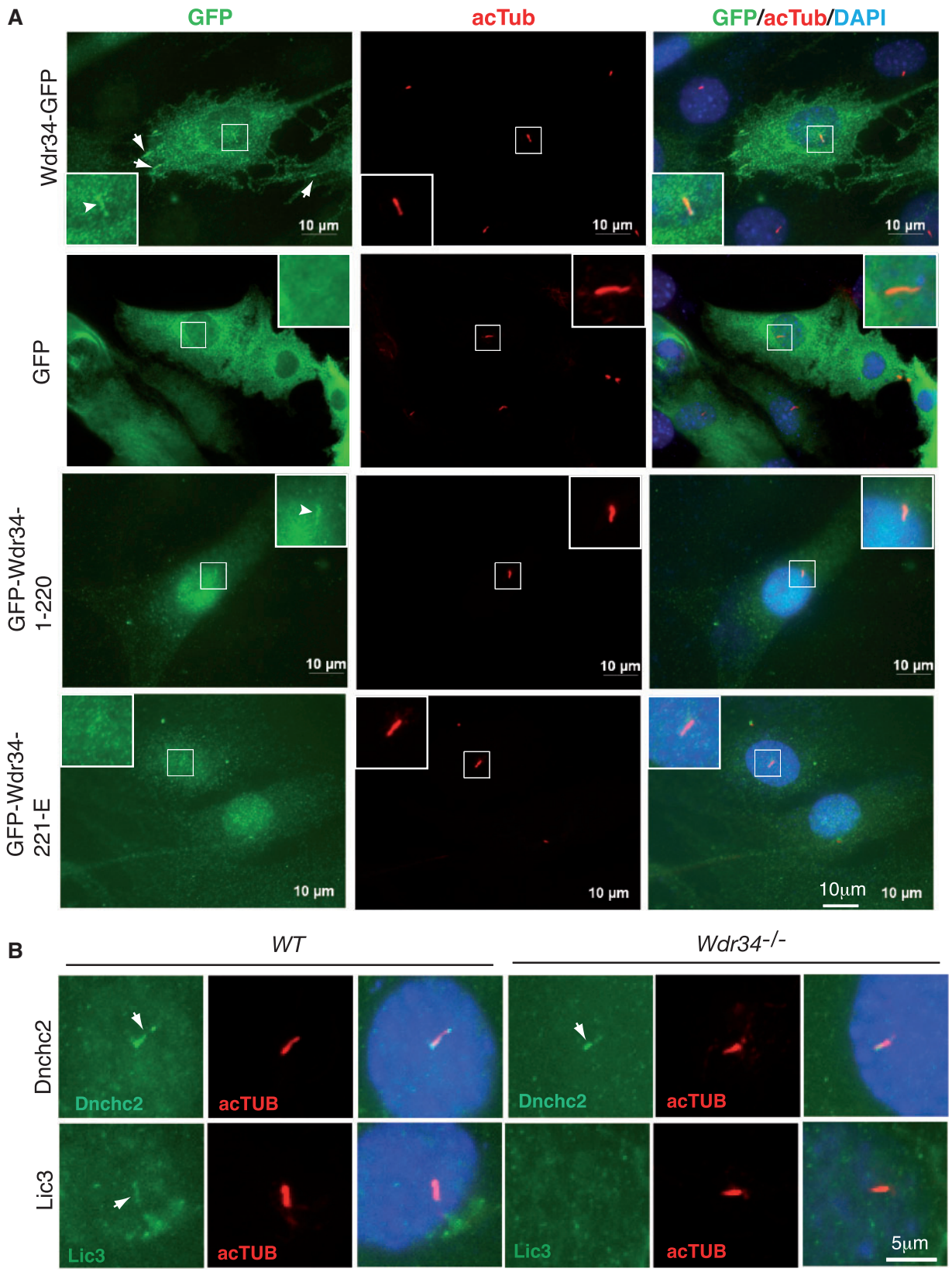

Figure 8. Wdr34 subcellular localization and its effect on Lic3 cilia localization. **(A)** Wild type MEFs stably expressing the indicated proteins were stained for GFP, acetylated tubulin (acTub), and nuclei (DAPI, blue). GFP-Wdr34 is occasionally enriched in cilia (12%, $n = 35$) and mostly accumulated in cell cortex and filopodia-like structure (indicated by arrows). Arrowheads indicate ciliary localization. **(B)** WT and *Wdr34* mutant MEFs were stained for the indicated proteins. Note that Lic3 is absent in the cilia of *Wdr34* mutant cells.

(Fig. 9, no treatment). To assess the microtubule growth rate, the cells were treated with nocodazole and then stained for microtubules after nocodazole removal for different period of time. Microtubules began to regrow in both wild type and mutant cells 5 min after nocodazole removal and grew slightly longer in the wild type than mutant cells in 10 min. The difference in microtubule regrowth between wild type and mutant cells became more pronounced by 20 min and remained at 60 min, albeit smaller (Fig. 9). Thus, loss of either *Wdr34* or *Dnchc2* results in a decrease in microtubule regrowth rate.

Discussion

Anterograde ciliary protein trafficking is powered by kinesin 2 motors, while retrograde ciliary protein trafficking is directed by cytoplasmic dynein 2 motor. A recent study showed that Wdr34 and Wdr60 are bona fide dynein 2 intermediate chains (16). Consistent with the specific role of dynein 2 in retrograde IFT trafficking in cilia, mutations in dynein heavy chain gene *Dnchc2* in both human and mouse result in stumpy cilia and aberrant accumulation of ciliary proteins in cilia (19,20,33). Similarly, mutations in human *WDR34* gene lead to stumpy cilia

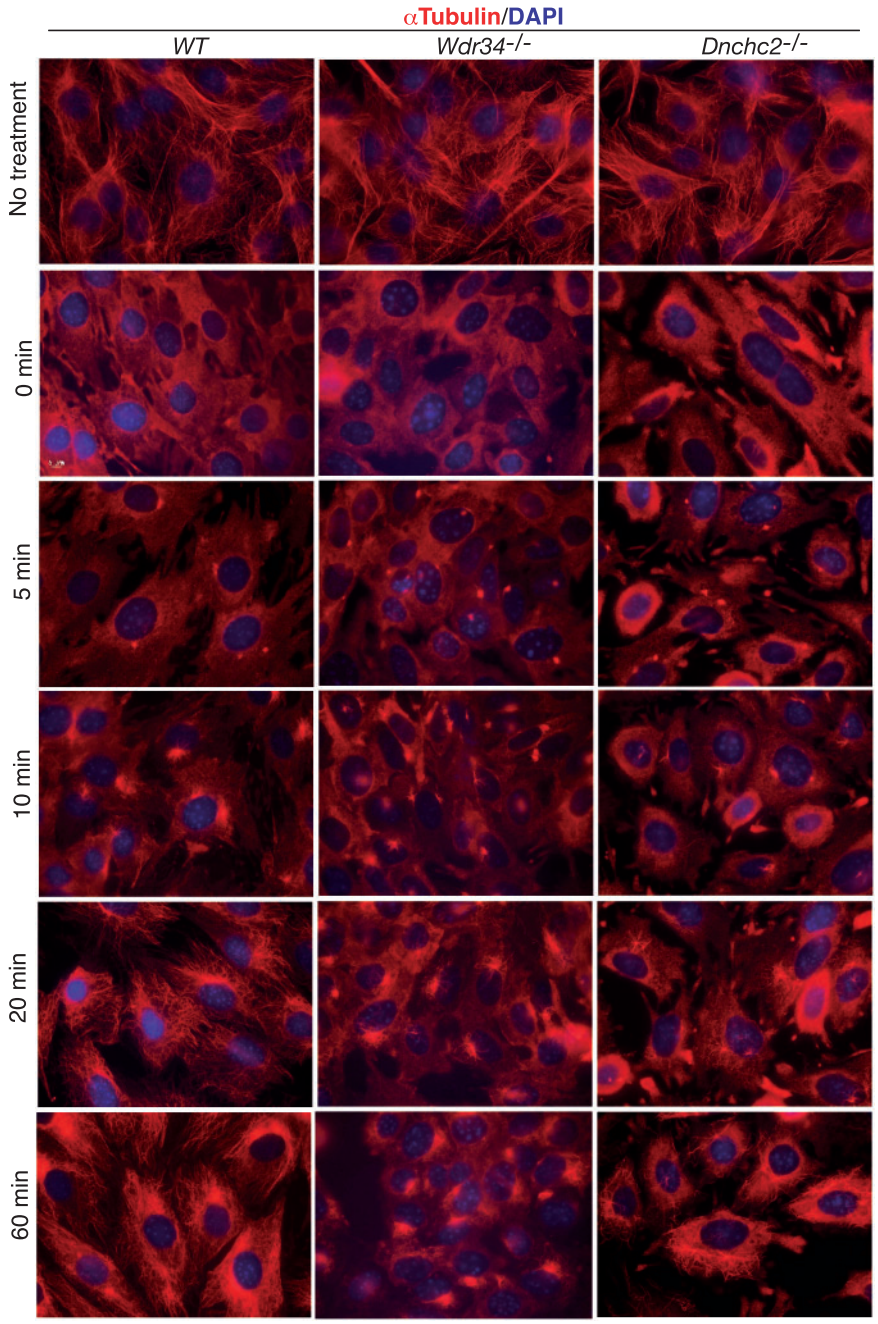

Figure 9. Microtubule regrowth delays in either *Wdr34* or *Dnchc2* mutant cells. Microtubules and nuclei were visualized with αtubulin (red) and DAPI (blue) staining, respectively. Wild type (wt), *Wdr34*, and *Dnchc2* mutant MEFs were treated with nocodazole. Microtubule regrowth was then assessed after nocodazole removal for the indicated times. Note that nocodazole treatment destroyed microtubule organization in both wt and mutant cells (0 min) and that microtubule regrowth delayed in both mutants as compared to wt.

(22,23). However, cilia defects in human *WDR34* mutant cells have not been completely characterized. In the present study, we show that like human *Wdr34* mutations, inactivation of the mouse *Wdr34* results in short and bulbous cilia. We also extend previous studies on human *WDR34* by showing that all the ciliary proteins examined, including Arl13b, Smo, Gli2, Gli3, Ift88, Ift57, and Ift140, accumulate abnormally at the cilia tip of both *Wdr34* and *Dnchc2* mutant cells (Figs 5 and 7). Together, these data indicate that as a part of dynein 2, Wdr34 is necessary for retrograde IFT trafficking.

It is worth noting that Arl13b and Smo staining areas in the mutant cilia are usually big and loose like 'cloud' as compared to those of IFT protein staining (Fig. 5C). This is most likely attributed to the fact that Arl13b and Smo are localized to ciliary membrane, while IFTs are associated with the microtubule shaft in the cilia. We also noticed that cilia number is similar in the tissues examined in wild type and *Wdr34* mutant embryos, but it is significantly reduced in the mutant MEFs as compared to that in wild type MEFs (Fig. 5B and C). This difference is most likely due to the difference between in vitro culture and in vivo physiological conditions that support ciliogenesis. It is also possible that since MEFs comprise only some cell types, cilia number in MEFs may not exactly represent that in embryos.

Hh signaling depends on cilia. Mutations in genes encoding kinesin motors, IFT components, dynein 2 heavy chain, and many other proteins have been shown to cause dysfunctional Hh signaling (6). Although human *WDR34* mutations have been recently shown to cause stumpy cilia (22,23), the link between *WDR34* and Hh signaling has not been established. Several pieces of evidence from the current study show that loss of *Wdr34* gene function disrupts Hh signaling downstream of Smo, but upstream of Gli2 and Gli3. First, all Shh-dependent ventral neural markers examined (Foxa2, Nkx2.2, Hb9 and Isl1) are missing in the *Wdr34* mutant neural tube. In contrast, the expression of Pax6 and Pax7, two dorsal markers inhibited by the high level of Hh signaling, is ventrally expanded (Fig. 2A). It is worth noting that unlike those in *Wdr34* mutant, Hb9 and Isl1 are expressed in the neural tube of *Dnchc2* mutants (20,33). This difference could be due to the difference in genetic background, potentially residual *Dnchc2* mutant gene function, and/or the role in Hh signaling between Wdr34 and Dnchc2. Second, the expression of *Ptch1-lacZ* and *Gli1*, two Hh targets, is inhibited in the *Wdr34* mutant neural tube and limb (Figs 2B and 3). Since the ventral neural tube patterning and the expression of the Hh targets are dependent on $Gli2^{FL}$ and $Gli3^{FL}$ activators, yet both $Gli2^{FL}$ and $Gli3^{FL}$ levels are remarkably elevated in the mutant (Fig. 4), these results indicate that $Gli2^{FL}$ and $Gli3^{FL}$ are inactive in the *Wdr34* mutant. Third, *Wdr34* mutant embryos exhibit open brain and neural tube and polydactyly (Fig. 1C and D), the phenotypes that are usually associated with increased Hh signaling (25,40–42). However, since both $Gli2^{FL}$ and $Gli3^{FL}$ are not activated, these mutant phenotypes are most likely due to the change in the $Gli3^{FL}$ to $Gli3^{Rep}$ ratio and/or reduced $Gli3^{Rep}$ function. Thus, as in *Dnchc2* mutants (19,20,33), both Gli2/Gli3 activator and repressor functions are impaired in *Wdr34* mutant. Lastly, loss of *Wdr34* gene function does not affect the additional enrichment of Smo in cilia in response to Hh stimulation. However, it does prevent Hh-dependent Gli2 and Gli3 accumulation in cilia. This is also true for *Dnchc2* mutations (Fig. 7). These results indicate that both Wdr34 and Dnchc2 act between Smo and Gli2/Gli3 in the Hh pathway.

Recent studies showed that endogenous Wdr34 is localized to the base of cilia, while GFP-tagged Wdr34 is also found in the cilia axoneme (16,23). We found GFP-Wdr34 localized to cilia only in a small fraction (12%) of MEFs stably overexpressing the fusion protein. In most of the cells, the protein appears to be enriched in cell cortices and filopodia-like structure. Similarly, GFP-Wdr34-1-220 also appears to be localized to cilia in some of GFP-Wdr34-1-220 expressing cells (Fig. 8A). This suggests that the N-terminus controls Wdr34 ciliary localization. The difference in Wdr34 localization of endogenous and overexpressed proteins from different studies could be due to different antibodies and/or cell lines used. We do not yet know whether non-ciliary localization is physiologically relevant to Wdr34 function. If it were, this would suggest that Wdr34 also functions in subcellular location(s) other than cilia. Further studies are necessary to investigate this possibility.

In addition, loss of Wdr34 appears to affect the ciliary localization of Lic3 but not Dnchc2 (Fig. 8B), suggesting that Wdr34 is required for Lic3 ciliary localization or protein stability. We could not distinguish between the two mechanisms, since we do not know whether Lic3 protein levels are reduced in *Wdr34* mutant MEFs due to the sensitivity of the Lic3 antibody. Nevertheless, our finding raises the possibility that the dynein 2 entire complex, rather than individual subunits, may determine the ciliary localization and/or protein stability of individual subunits. This might also in part explain why overexpressed Wdr34 is mainly localized to the cytoplasm rather than cilia, as the amount of other subunits of the endogenous dynein 2 complex is limited.

Dynein 2 is considered to be a cilia specific motor for IFT retrograde trafficking. It is unknown whether dynein 2 plays any role in cytoplasmic microtubule network and dynamics. Our microtubule regrowth assay shows that the microtubules grow slower in *Wdr34* and *Dnchc2* mutant cells than that in wild type, although the microtubule network appears similar (Fig. 9). This suggests that dynein 2 promotes cytoplasmic microtubule growth. To our knowledge, this is the first piece of evidence that dynein 2 plays a role in a non-ciliary structure. Additional studies are necessary to elucidate the mechanism underlying this novel role of dynein 2.

Materials and Methods

Mouse strains and the generation of a *Wdr34* mutant allele

Institutional Animal Care and Use Committee at Weill Cornell Medical College approved this research including the use of mice and mouse embryonic fibroblasts.

A BAC clone containing mouse *Wdr34* genomic DNA sequences was purchased from the BACPAC Resources Center (Oakland, CA, USA) and used to create a *Wdr34* targeting construct. The construct was engineered by replacing exons 3–8 of the *Wdr34* gene with the neomycin cassette flanked by loxP sites (Fig. 1A). The linearized construct was electroporated into W4 ES cells, and targeted ES cell clones were identified by digestion of genomic DNA with BamHI, followed by a Southern blot analysis of ES cell DNA using a probe as indicated (Fig. 1B). Two *Wdr34*-targeted ES cell clones were injected into C57BL/6 blastocysts to generate chimeric founders, which were then bred with C57BL/6 to establish F1 heterozygotes. The *Wdr34* heterozygotes were maintained in 129/SVE, C57BL/6, and SW mix background. PCR (polymerase chain reaction) analysis was used for routine genotyping with the following primers: forward primer BW1221F, 5'-TACCTCACTGCAGCTCTCTCA-3' and reverse prime BW1221R, 5'-GTTGTACATCACCTGCAGGGA-3' for the wild type allele, which produced a 200 bp fragment; and forward primer

BW294, 5'-ATTGGGAAGACAATAGCAGGCA-3'and reverse primer BW1221R for the targeted *Wdr34* allele, which produced a 280 bp fragment.

Cell lines and cell culture

Wild type and mutant *Wdr34* primary mouse embryonic fibroblasts (pMEFs) were prepared from E11.5 or E12.5 mouse embryos. The procedure was approved by the Institutional Animal Care and Use Committee at Weill Medical College. The pMEFs were cultured in DMEM supplemented with 10% FBS (fetal bovine serum), penicillin, and streptomycin.

cDNA constructs, cloning, and transfection

To create GFP-Wdr34 or its mutant cDNA constructs, EGFP was first inserted into pLNCX retroviral vector (Clontech) by PCR and general cloning techniques. Mouse *Wdr34* cDNA was amplified from a mouse cDNA library and cloned in-frame into pLNCX-EGFP. Wdr34-1-220 (amino acid residues) and Wdr34-221-E (221aa to the C-terminal end) fragments were amplified and cloned in-frame into the same vector. The constructs were verified by DNA sequencing. Virus carrying GFP, GFP-Wdr34, or its mutant constructs were generated by cotransfecting each of the viral constructs with pEco construct into Phoenix-Eco cells (ATCC) using the calcium phosphate precipitation method (31).

To generate MEFs that stably expressed GFP-Wdr34, GFP-Wdr34-1-220, or GFP-Wdr34-221-E, wild type MEFs were transduced with the above virus. About 36 hours after transduction, the cells were incubated in the medium with G418 (1 mg/ml) until neomycin resistant clones emerged. Heterogeneous stable cells were maintained in the medium with 0.1 mg/ml G418.

Embryo section immunofluorescence and whole mount *in situ* hybridization

For immunofluorescence of neural tube sections, mouse embryos at 10.5 days post coitus (E10.5) were dissected, fixed in 4% paraformaldehyde (PFA)/PBS for 1 h at 4 °C, equilibrated in 30% sucrose/PBS overnight at 4 °C, and embedded in OCT. The frozen embryos were transversely cryosectioned at the forelimb areas (10 μm/section). Tissue sections were immunostained using antibodies against Shh, Foxa2 (concentrated), Nkx2.2, Hb9, Isl1/2, Pax6, and Pax7 (Developmental Study Hybridoma Bank (DSHB), Iowa), or Arl13b and acetylated αtubulin together as described (41). Whole mount in situ hybridization of mouse embryos with digoxigenin-labeled riboprobes was performed as described (43).

Cell immunofluorescence and microscopy

For cell ciliation studies, cells were plated on coverslips coated with 0.1% gelatin for at least overnight and serum starved with 0.1% FBS for 24 h to arrest the cells. To assess Smo, Gli2, and Gli3 ciliary localization in response to Hh signaling, MEFs were incubated with control or ShhN conditioned medium (1:10 dilution with DMEM medium, ShhN working concentration $\geq$ 5 nM, 1% FBS final concentration) overnight before immunostaining. ShhN conditioned medium was collected from HEK293 cells transfected with pRK-ShhN expression vector. ShhN level was initially estimated by Western blot, and its activity was initially determined by Gli-luciferase reporter assay using Shh-light cells (44). For centrosome staining, cells were fixed in −20 °C cold methanol for 5 min. For the cytoplasmic and cilia staining, cells were fixed in 4% PFA/PBS for 15 min. After wash with PBS, the cells were incubated with blocking solution (PBS/0.2% Triton X-100/4% heat inactivated calf serum) for 20 min. The cells were then incubated with primary antibodies in blocking solution for 1 h at room temperature. The cells were washed with PBS, incubated with secondary antibodies in blocking solution for 1 h at room temperature. After wash three times with PBS, the coverslips were mounted to glass slides with Vectashield mounting fluid with DAPI (Vector Labs). The staining was visualized using a Zeiss Axiovert fluorescent microscope.

Antibodies

Arl13b antibodies were generated by Covance, Inc. Rabbits were immunized with an insoluble His-tagged mouse Arl13b purified from bacteria. It was used in a 1:1000 dilution. Other antibodies include: Smo (1:1000) (11), Gli2, Gli3, Ift88, Cep164, Odf2, Ta3, Cep290, GFP, Dnchc2, Lic3 (all 1:1000) (31,37,39), acetylated tubulin (1:4000), γ−tubulin (1:4000) (Sigma), Ift57 (1:1000), and IFT40 (1:1000) (45). Secondary antibodies Alexa Fluor 488-conjugated donkey anti-rabbit IgG and Cy3-conjugated donkey anti-mouse IgG were purchased from Jackson Immunoresearch, Inc.

Immunoblotting

E10.5 mouse embryos were washed with PBS and lysed in RIPA buffer (50 mM Tris-HCl [pH 7.4], 150 mM NaCl, 1 mM EDTA, 1%Triton X-100, 1% sodium deoxycholate, 0.1% SDS, protease inhibitors) for 10 min on ice. After being cleared by centrifugation, the lysates were mixed with protein loading buffer, resolved in SDS polyacrylamide gel, and transferred to a nitrocellulose membrane followed by western blotting as described (5).

Scanning electron microscopy

E9.5 wild type and *Wdr34* mutant embryos were fixed with 2% paraformaldehyde/2% glutaraldehyde in 0.075 M sodium cacodylate buffer (EM quality) overnight at room temperature. After wash with PBS, the embryos were dissected to expose the lumen of the neural tube. The embryo fragments were dehydrated using a series of graded ethanol and subjected to critical point drying. The embryo fragments were mounted with the lumen faced-up on aluminum stubs with adhesive tabs and sputter-coated with gold-palladium alloy. Cilia of neural epithelia in the neural tube were imaged using a field emission electron microscope (Supra 25; Carl Zeiss).

Microtubule regrowth assay

MEFs were seeded onto coverslips coated with 0.1% gelatin in growth medium. After 24 h, they were treated with 1μg/ml nocodazole for 1h at 37 °C. The cells were washed once, incubated with normal growth medium to allow microtubule regrow and then fixed at 0, 5, 10, 20, and 60 min after nocodazole treatment, using −20 °C cold methanol. The cells were stained with αtubulin and DAPI and imaged.

Acknowledgements

We thank Dr. Gregory Pazour for Ift57 and Ift140 antibodies, Dr. Rajat Rohatgi for Smo antibody, Dr. Richard Vallee for Dnchc2

and Lic3 antibodies. We also thank Ms. Nina Lampen for assistance with SEM. Shh, Isl1, Hb9, Pax6, Pax7, Nkx2.2, and Foxa2 monoclonal antibodies were purchased from the Developmental Studies Hybridoma Bank maintained by the University of Iowa, Department of Biological Sciences, Iowa City, Iowa 52242, under contract NO1-HD-7-3263 from the NICHD. Procedures involved in mice were performed under an approved animal protocol. B.W. was supported by a National Institutes of Health, USA and K.T. and C.W. were supported by the Chinese Natural Science Foundation.

Conflict of Interest statement. None declared.

Funding

National Institutes of Health, USA (grant R01GM114429) and Chinese Natural Science Foundation (grant 81172294 and 81600401).

References

1. Jiang, J. and Hui, C.C. (2008) Hedgehog signaling in development and cancer. *Dev. Cell*, **15**, 801–812.
2. Fuse, N., Maiti, T., Wang, B., Porter, J.A., Hall, T.M., Leahy, D.J. and Beachy, P.A. (1999) Sonic hedgehog protein signals not as a hydrolytic enzyme but as an apparent ligand for patched. *Proc. Natl. Acad. Sci. U. S. A*, **96**, 10992–10999.
3. Stone, D.M., Hynes, M., Armanini, M., Swanson, T.A., Gu, Q., Johnson, R.L., Scott, M.P., Pennica, D., Goddard, A., Phillips, H., Noll, M., Hooper, J.E. *et al.* (1996) The tumour-suppressor gene patched encodes a candidate receptor for Sonic Hedgehog. *Nature*, **384**, 129–134.
4. Pan, Y., Bai, C.B., Joyner, A.L. and Wang, B. (2006) Sonic Hedgehog signaling regulates Gli2 transcriptional activity by suppressing its processing and degradation. *Mol. Cell. Biol.*, **26**, 3365–3377.
5. Wang, B., Fallon, J.F. and Beachy, P.A. (2000) Hedgehog-regulated processing of Gli3 produces an anterior/posterior repressor gradient in the developing vertebrate limb. *Cell*, **100**, 423–434.
6. Goetz, S.C. and Anderson, K.V. (2010) The primary cilium: a signalling centre during vertebrate development. *Nat. Rev.* **11**, 331–344.
7. Corbit, K.C., Aanstad, P., Singla, V., Norman, A.R., Stainier, D.Y. and Reiter, J.F. (2005) Vertebrate Smoothened functions at the primary cilium. *Nature*, **437**, 1018–1021.
8. Endoh-Yamagami, S., Evangelista, M., Wilson, D., Wen, X., Theunissen, J.W., Phamluong, K., Davis, M., Scales, S.J., Solloway, M.J., de Sauvage, F.J. and Peterson, A.S. (2009) The mammalian Cos2 homolog Kif7 plays an essential role in modulating Hh signal transduction during development. *Curr. Biol.*, **19**, 1320–1326.
9. Haycraft, C.J., Banizs, B., Aydin-Son, Y., Zhang, Q., Michaud, E.J. and Yoder, B.K. (2005) Gli2 and Gli3 localize to cilia and require the intraflagellar transport protein polaris for processing and function. *PLoS Genet.*, **1**, e53.
10. Liem, K.F., Jr., He, M., Ocbina, P.J. and Anderson, K.V. (2009) Mouse Kif7/Costal2 is a cilia-associated protein that regulates Sonic Hedgehog signaling. *Proc. Natl. Acad. Sci. U. S. A*, **106**, 13377–13382.
11. Rohatgi, R., Milenkovic, L. and Scott, M.P. (2007) Patched1 regulates Hedgehog signaling at the primary cilium. *Science*, **317**, 372–376.
12. Quinlan, R.J., Tobin, J.L. and Beales, P.L. (2008) Modeling ciliopathies: Primary cilia in development and disease. *Curr. Top. Dev. Biol.*, **84**, 249–310.
13. Pedersen, L.B. and Rosenbaum, J.L. (2008) Intraflagellar transport (IFT) role in ciliary assembly, resorption and signalling. *Curr. Top. Dev. Biol.*, **85**, 23–61.
14. Silverman, M.A. and Leroux, M.R. (2009) Intraflagellar transport and the generation of dynamic, structurally and functionally diverse cilia. *Trends Cell Biol.*, **19**, 306–316.
15. Scholey, J.M. (2013) Kinesin-2: a family of heterotrimeric and homodimeric motors with diverse intracellular transport functions. *Annu. Rev. Cell Dev. Biol.*, **29**, 443–469.
16. Asante, D., Stevenson, N.L. and Stephens, D.J. (2014) Subunit composition of the human cytoplasmic dynein-2 complex. *J. Cell Sci.*, **127**, 4774–4787.
17. Pfister, K.K., Shah, P.R., Hummerich, H., Russ, A., Cotton, J., Annuar, A.A., King, S.M. and Fisher, E.M. (2006) Genetic analysis of the cytoplasmic dynein subunit families. *PLoS Genet.*, **2**, e1.
18. Rajagopalan, V., D'Amico, J.P. and Wilkes, D.E. (2013) Cytoplasmic dynein-2: from molecules to human diseases. *Front. Biol.*, 1–8.
19. Huangfu, D. and Anderson, K.V. (2005) Cilia and Hedgehog responsiveness in the mouse. *Proc. Natl. Acad. Sci. U. S. A*, **102**, 11325–11330.
20. May, S.R., Ashique, A.M., Karlen, M., Wang, B., Shen, Y., Zarbalis, K., Reiter, J., Ericson, J. and Peterson, A.S. (2005) Loss of the retrograde motor for IFT disrupts localization of Smo to cilia and prevents the expression of both activator and repressor functions of Gli. *Dev. Biol.*, **287**, 378–389.
21. Okamoto, T., Nagaya, K., Kawata, Y., Asai, H., Tsuchida, E., Nohara, F., Okajima, K. and Azuma, H. (2014) Novel compound heterozygous mutations in DYNC2H1 in a patient with severe short-rib polydactyly syndrome type III phenotype. *Congenit. Anom. (Kyoto)*, **55**, 155–157.
22. Huber, C., Wu, S., Kim, A.S., Sigaudy, S., Sarukhanov, A., Serre, V., Baujat, G., Le Quan Sang, K.H., Rimoin, D.L., Cohn, D.H., Munnich, A., Krakow, D. *et al.* (2013) WDR34 mutations that cause short-rib polydactyly syndrome type III/severe asphyxiating thoracic dysplasia reveal a role for the NF-kappaB pathway in cilia. *Am. J. Hum. Genet.*, **93**, 926–931.
23. Schmidts, M., Vodopiutz, J., Christou-Savina, S., Cortes, C.R., McInerney-Leo, A.M., Emes, R.D., Arts, H.H., Tuysuz, B., D'Silva, J., Leo, P.J., Giles, T.C., Oud, M.M. *et al.* (2013) Mutations in the gene encoding IFT dynein complex component WDR34 cause Jeune asphyxiating thoracic dystrophy. *Am. J. Hum. Genet.*, **93**, 932–944.
24. Briscoe, J., Pierani, A., Jessell, T.M. and Ericson, J. (2000) A homeodomain protein code specifies progenitor cell identity and neuronal fate in the ventral neural tube. *Cell*, **101**, 435–445.
25. Goodrich, L.V., Milenkovic, L., Higgins, K.M. and Scott, M.P. (1997) Altered neural cell fates and medulloblastoma in mouse patched mutants. *Science*, **277**, 1109–1113.
26. Litingtung, Y., Dahn, R.D., Li, Y., Fallon, J.F. and Chiang, C. (2002) Shh and Gli3 are dispensable for limb skeleton formation but regulate digit number and identity. *Nature*, **418**, 979–983.
27. te Welscher, P., Fernandez-Teran, M., Ros, M.A. and Zeller, R. (2002) Mutual genetic antagonism involving GLI3 and dHAND prepatterns the vertebrate limb bud mesenchyme prior to SHH signaling. *Genes Dev.*, **16**, 421–426.
28. te Welscher, P., Zuniga, A., Kuijper, S., Drenth, T., Goedemans, H.J., Meijlink, F. and Zeller, R. (2002) Progression of vertebrate limb development through SHH-mediated counteraction of GLI3. *Science*, **298**, 827–830.

29. Zuniga, A., Haramis, A.P., McMahon, A.P. and Zeller, R. (1999) Signal relay by BMP antagonism controls the SHH/FGF4 feedback loop in vertebrate limb buds. *Nature*, **401**, 598–602.
30. Martin, G.R. (1998) The roles of FGFs in the early development of vertebrate limbs. *Genes Dev.*, **12**, 1571–1586.
31. Wang, C., Low, W.C., Liu, A. and Wang, B. (2013) Centrosomal protein DZIP1 regulates Hedgehog signaling by promoting cytoplasmic retention of transcription factor GLI3 and affecting ciliogenesis. *J. Biol. Chem.*, **288**, 29518–29529.
32. Caspary, T., Larkins, C.E. and Anderson, K.V. (2007) The graded response to Sonic Hedgehog depends on cilia architecture. *Dev. Cell*, **12**, 767–778.
33. Ocbina, P.J., Eggenschwiler, J.T., Moskowitz, I. and Anderson, K.V. (2011) Complex interactions between genes controlling trafficking in primary cilia. *Nat. Genet.*, **43**, 547–553.
34. Graser, S., Stierhof, Y.D., Lavoie, S.B., Gassner, O.S., Lamla, S., Le Clech, M. and Nigg, E.A. (2007) Cep164, a novel centriole appendage protein required for primary cilium formation. *J. Cell Biol.*, **179**, 321–330.
35. Nakagawa, Y., Yamane, Y., Okanoue, T., Tsukita, S. and Tsukita, S. (2001) Outer dense fiber 2 is a widespread centrosome scaffold component preferentially associated with mother centrioles: its identification from isolated centrosomes. *Mol. Biol. Cell*, **12**, 1687–1697.
36. Valente, E.M., Silhavy, J.L., Brancati, F., Barrano, G., Krishnaswami, S.R., Castori, M., Lancaster, M.A., Boltshauser, E., Boccone, L., Al-Gazali, L., Fazzi, E., Signorini, S. *et al.* (2006) Mutations in CEP290, which encodes a centrosomal protein, cause pleiotropic forms of Joubert syndrome. *Nat. Genet.*, **38**, 623–625.
37. Wu, C., Yang, M., Li, J., Wang, C., Cao, T., Tao, K. and Wang, B. (2014) Talpid3-binding centrosomal protein Cep120 is required for centriole duplication and proliferation of cerebellar granule neuron progenitors. *PloS One*, **9**, e107943.
38. Yin, Y., Bangs, F., Paton, I.R., Prescott, A., James, J., Davey, M.G., Whitley, P., Genikhovich, G., Technau, U., Burt, D.W. and Tickle, C. (2009) The Talpid3 gene (KIAA0586) encodes a centrosomal protein that is essential for primary cilia formation. *Development*, **136**, 655–664.
39. Mikami, A., Tynan, S.H., Hama, T., Luby-Phelps, K., Saito, T., Crandall, J.E., Besharse, J.C. and Vallee, R.B. (2002) Molecular structure of cytoplasmic dynein 2 and its distribution in neuronal and ciliated cells. *J. Cell Sci.*, **115**, 4801–4808.
40. Cooper, A.F., Yu, K.P., Brueckner, M., Brailey, L.L., Johnson, L., McGrath, J.M. and Bale, A.E. (2005) Cardiac and CNS defects in a mouse with targeted disruption of suppressor of fused. *Development*, **132**, 4407–4417.
41. Pan, Y., Wang, C. and Wang, B. (2009) Phosphorylation of Gli2 by protein kinase A is required for Gli2 processing and degradation and the Sonic Hedgehog-regulated mouse development. *Dev. Biol.*, **326**, 177–189.
42. Svard, J., Heby-Henricson, K., Persson-Lek, M., Rozell, B., Lauth, M., Bergstrom, A., Ericson, J., Toftgard, R. and Teglund, S. (2006) Genetic elimination of Suppressor of fused reveals an essential repressor function in the mammalian Hedgehog signaling pathway. *Dev. Cell*, **10**, 187–197.
43. Wang, C., Pan, Y. and Wang, B. (2007) A hypermorphic mouse Gli3 allele results in a polydactylous limb phenotype. *Dev. Dyn.*, **236**, 769–776.
44. Taipale, J., Chen, J.K., Cooper, M.K., Wang, B., Mann, R.K., Milenkovic, L., Scott, M.P. and Beachy, P.A. (2000) Effects of oncogenic mutations in Smoothened and Patched can be reversed by cyclopamine. *Nature*, **406**, 1005–1009.
45. Pazour, G.J., Baker, S.A., Deane, J.A., Cole, D.G., Dickert, B.L., Rosenbaum, J.L., Witman, G.B. and Besharse, J.C. (2002) The intraflagellar transport protein, IFT88, is essential for vertebrate photoreceptor assembly and maintenance. *J. Cell Biol.*, **157**, 103–113.